Available online at www.sciencedirect.com

ScienceDirect

Proceedings of the Combustion Institute 38 (2021) 6533–6540

Proceedings of the Combustion Institute

www.elsevier.com/locate/proci

Time-resolved *in situ* measurements and predictions of plasma-assisted methane reforming in a nanosecond-pulsed discharge

Timothy Y. Chen [a,*], Taaresh S. Taneja [b], Aric C. Rousso [a], Suo Yang [b], Egemen Kolemen [a], Yiguang Ju [a]

[a] *Department of Mechanical and Aerospace Engineering, Princeton University, Princeton, NJ 08544, USA*
[b] *Department of Mechanical Engineering, University of Minnesota–Twin Cities, Minneapolis, MN 55455, USA*

Received 7 November 2019; accepted 10 June 2020
Available online 26 September 2020

Abstract

This study investigates the plasma properties and chemical kinetics of plasma-assisted methane reforming in a He diluted nanosecond-pulsed plane-to-plane dielectric barrier discharge (ns-DBD) through the combination of time-resolved *in situ* laser diagnostics and a 1-D numerical model. Plasma-assisted fuel reforming kinetic mechanisms have predominantly been evaluated on the basis of matching reactant conversion and syngas production to steady-state measurements, which cannot describe the full range of chemistry and physics necessary to validate the model. It was found that adding 1% CH_4 to a pure He ns-DBD led to a faster breakdown along the rising edge of the applied voltage pulse, thereby lowering the reduced electric field (E/N), electron number density, and electron temperature. Further addition of CH_4 did not continue to alter the E/N in the model. Laser absorption spectroscopy was used to measure gas temperature, C_2H_2, H_2O, and CH_2O in a CH_4/CO_2/He discharge to serve as validation targets for the predicted reaction pathways. CH_2O was predicted within 25% of the measured value, while H_2O and C_2H_2 were under-predicted by a factor of two and three, respectively. From path flux analysis, the major pathway for CH_2O formation was through the reaction between CH_3 and O, while C_2H_2 formation had multi-step pathways that relied on ions like CH_3^+ and $C_2H_5^+$. The path flux analysis also shows that CH_2 is a significant intermediate for production of both CH_2O and C_2H_2, and increased CH_2 concentration could improve model predictions. The results show that the use of reaction rate constants with lower uncertainties and inclusion of He_2^+ are needed to improve the predictions. Finally, varying the "equivalence ratio", defined by the CH_4 dry reforming reaction to H_2 and CO, from 0.5 to 2 was shown to have a weak effect on measured product species and experimental trends were explained based on pathways extracted from the model.

Keywords: Non-equilibrium plasma; Plasma assisted fuel reforming; Chemical kinetics; Methane dry reforming; Pyrolysis

* Corresponding author.
E-mail address: tc8@princeton.edu (T.Y. Chen).

https://doi.org/10.1016/j.proci.2020.06.100
1540-7489

1. Introduction

There has been growing interest in utilizing plasma for conversion of methane into value-added products, since non-equilibrium plasmas have been previously demonstrated to significantly enhance the chemical reactivity of the gas mixture through generation of radicals and excited species, allowing for production of liquid chemicals near room temperature when paired with catalysts [1]. Plasmas can be operated "on-demand" and be configured in a modular fashion, making them a compelling alternative to traditional thermal reforming method for processing excess methane (the major component of natural gas) at oil-production sites that would otherwise be flared [2]. In 2018, 145 billion cubic meters of natural gas were flared and represented almost 4% of natural gas produced in the same year [2,3]. Assuming the flared gas was burned completely, that translates to 0.7% of global CO_2 emissions in 2018 [4]. Therefore, plasma-assisted reforming of methane has the potential to make a significant impact on reducing greenhouse gas emissions, particularly if CO_2 is used as the oxidizer, and has been studied for the past several decades [5,6].

While significant progress has been made in developing detailed kinetic mechanisms and multi-scale modeling for plasma-assisted combustion [7], the key reaction pathways for plasma-assisted fuel reforming are not well understood. Most experimental plasma-assisted fuel reforming studies focus on achieving the maximum selectivity, energy efficiency, and conversion of reactants rather than studying the plasma-chemical kinetics. The primary measurement method for these studies is *ex situ* steady-state gas chromatography (GC). For example, in Ref. [8], plasma-assisted dry reforming was studied using repetitively pulsed nanosecond pulsed plasma with bare metal electrodes, and higher energy efficiency relative to other types of discharges was reported. In Ref. [9], operating parameters in a cylindrical nanosecond-pulsed dielectric barrier discharge (ns-DBD) were varied, and it was reported that fast rise and fall of applied voltage and high pulse repetition frequencies led to an increase in energy efficiency and reactant conversion. Instead of conducting many experiments in a trial-and-error manner, developing a validated predictive model would be more efficient for optimization and provide deeper scientific insights to the underlying physics and chemistry.

Due to the limited number of *in situ* time-resolved measurements in the literature, plasma-assisted fuel reforming kinetic models are predominantly validated by GC measurements of reactant conversion and production of syngas (CO and H_2) [10]. However, in a CH_4 plasma-assisted oxidation study [11], the model predicted the GC measurements well but under-predicted CH_2O by a factor of four. In a plasma-assisted n-heptane oxidation study [12], an under-prediction of CH_2O by a factor of 40 was reported. If the kinetics for intermediate species are not predicted well, then it would be difficult to trust the modeling results in new applications without conducting additional validation experiments. Therefore, there is a critical need for time-resolved *in situ* measurements, in a simple plasma geometry with a controlled flow, to provide validation targets for numerical modeling so that the main reaction pathways can be understood.

In this study, time-resolved temperature, CH_2O, C_2H_2, and H_2O measurements of plasma-assisted CH_4 pyrolysis and dry reforming diluted with He are conducted using laser absorption spectroscopy in a ns-DBD flow reactor [11–13]. The equivalence ratio of CH_4 and CO_2 was varied with the amount of He dilution held constant to understand the sensitivity of the equivalence ratio on selectivity toward the measured products. These measurements are then compared against a one-dimensional (1-D) numerical model using a kinetic mechanism from the literature that was previously validated against GC measurements to validate the predictions and reveal areas for improvement [14]. Additional validation targets for electron number density (n_e) and temperature (T_e) in a CH_4/He ns-DBD [15] were used for evaluating the plasma physics predictions by the model and to understand the trends observed in that study.

2. Experimental methods

The experimental setup has been discussed previously in the literature [11,12] and is described briefly here. The plasma flow reactor was a plane-to-plane dielectric barrier discharge with a gap distance of 14 mm and 44.5 mm square metal electrodes. The pressure was set to 60 Torr via a needle valve and the overall flow velocity was 0.2 m/s, which was sufficiently low to remove flow effects. Mass flow controllers (MKS) were used to set the gas flow rates of CH_4, CO_2, and He. Equivalence ratios (ϕ) of 0.5, 1, and 2 were used in this study with the He dilution held constant at 70%. The equivalence ratio was defined by the methane dry reforming reaction of $CH_4+CO_2 \rightarrow 2H_2+2CO$ with CO_2 treated as the oxidizer. The pyrolysis mixture was 15% CH_4 / 85% He, which was the same concentration of CH_4 in the stoichiometric dry reforming case. A nanosecond-pulse power supply (FID GmBH FPG 30-50MC4) generated the voltage pulses with a repetition frequency of 30 kHz, a full width at half maximum (FWHM) of 12 ns, and a peak voltage of 32 kV. The power supply was triggered using a function generator (SRS DS345) in a burst mode with a burst frequency of 2 Hz which flushed the plasma volume with new gas between bursts. The pulse repetition frequency was 30 kHz with 300 pulses applied in a burst. The peak voltage was measured to be approximately 10

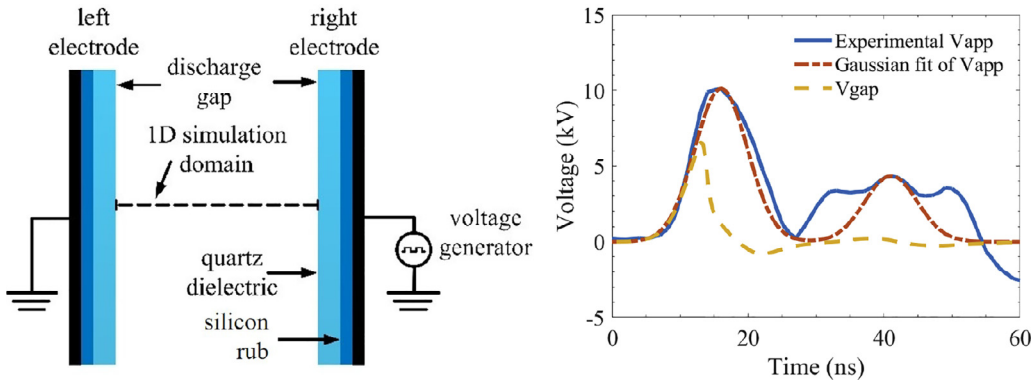

Fig. 1. Physical configuration of the 1-D simulation and Gaussian fit of experimental pulse waveform of applied voltage (Vapp) used in simulation and the resulting gap voltage (Vgap).

kV. An external-cavity quantum cascade laser (EC-QCL, Daylight Solutions 21074-MHF) scanned CH_4, C_2H_2, and H_2O absorption lines. The C_2H_2 and H_2O lines are located at 1321.03 cm^{-1} and 1312.55 cm^{-1}, respectively. CH_4 absorption lines at 1343.56 cm^{-1} and 1343.63 cm^{-1} were used for the two absorption line temperature measurement, as described in Ref. [16]. A distributed feedback quantum cascade laser (DFB QCL, Alpes Lasers sbcw3176) measured CH_2O at 1726.9 cm^{-1}. The two lasers enter a 24-pass Herriott cell in the flow reactor before reaching the detector. All laser absorption data was fit with simulated spectra using the HITRAN database [17]. A 50.8 mm germanium etalon was used to determine the frequency axis. The measurement uncertainty was estimated to be 10% for CH_2O and 20% for C_2H_2 and H_2O, while the uncertainty for the temperature measurement was 10 K.

Thomson scattering is an *in situ* laser diagnostic that measures electron number density (n_e) and electron temperature (T_e) simultaneously [15]. The Thomson scattering measurements were used as model validation targets alongside the species measurements in the plasma flow reactor. The gas mixture used was 0–2% CH_4 added to a He bath gas in a ns-DBD pulsed at a 100 Hz continuous repetition frequency.

3. Numerical methods

The 1-D model in this study is adopted from Yang et al. [7,13,18]. The physical configuration of the plane-to-plane dielectric barrier discharge is shown in Fig. 1 with the 1-D simulation domain being marked as a dashed line. The computational domain is set to be from the left electrode to the right electrode, with the right electrode connecting to a high voltage power supply, and the left electrode being grounded. Each electrode is covered with dielectric layers, with the gas mixture filling the gap between dielectrics. The dielectric constants are fixed (4.8 for quartz and 3.2 for silicone rubber) for all simulations in the present work. Gaussian voltage pulses fitted from the experimental measurement of applied voltage (Vapp) are applied, as shown in Fig. 1. Governing equations include the Poisson's equation of electric potential, equation of electron energy, transport equations of both charged and neutral species, and conservation equations of mass, momentum, and energy, which are solved simultaneously. In particular, by solving the 1-D Poisson's equation of electric potential, the breakdown of the gas mixture can be accurately captured as the sharp drop of gap voltage (Vgap) in Fig. 1. In addition to the electron-impact reaction rate coefficients, the electron transport coefficients are also expressed as functions of electron energy by BOLSIG [19], and are updated through interpolation during every time step. The plasma drift-diffusion fluid model with the local electron mean energy approximation is applied for the transport of plasma species and energy [20].

Wang et al. [14] was used as the base mechanism for the chemical kinetics in the 1-D model, and the Helium mechanism was updated with additional reactions from Ref. [21]. To speed up computation time, the kinetic mechanisms were reduced by removing reactions involving species such as O_2 and O_3 and several electron-impact processes such as vibrational excitation of CH_4. These reductions are not expected to significantly alter the chemical kinetics, as vibrational excitation is inefficient for the E/N used in this discharge and would not significantly enhance dissociation. O_2 and O_3 can be neglected since these species can only be directly produced by 3-body recombination with O radicals or dissociative recombination of CO_2^+. Both of these channels are expected to be minor due to the low electron number density, on the order of 10^{12} cm−3, and low pressure of 60 Torr.

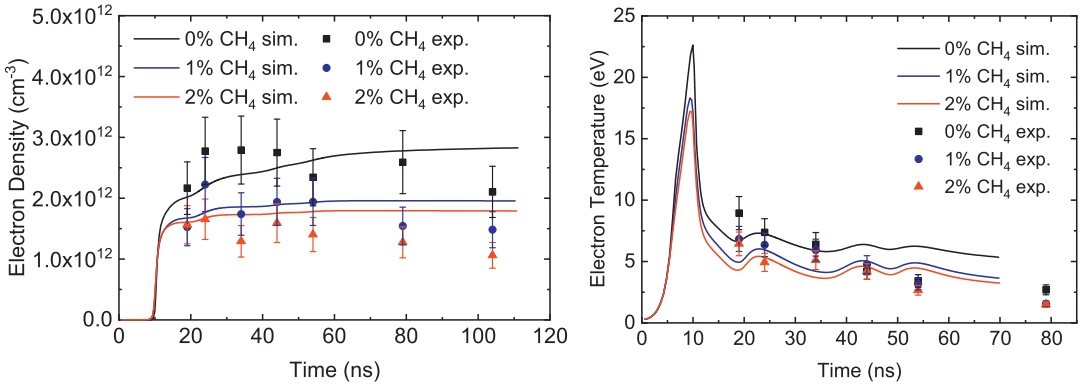

Fig. 2. Predicted (this work) and measured (Ref. [15]) time evolution of electron number density (n_e) and electron temperature (T_e) for 0–2% CH_4 addition to He ns-DBD.

4. Results and discussion

4.1. Prediction and validation of electron number density and temperature

Previously measured data from Ref. [15] was used to validate the predictions for electron number density (n_e) and electron temperature (T_e) in a He ns-DBD with 0–2% CH_4 addition. The measured applied voltage waveform was Gaussian fitted and input into the model. The experiment was approximated in the model as a single pulse, due to the long inter-pulse time in the 100 Hz discharge that was previously measured. The results of the simulation were overlaid with the experimental measurements in Fig. 2.

The overall trend and magnitude of the electron number density were well predicted during the first forty nanoseconds. However, there was a discrepancy in the afterglow where the experimental electron number density decays, while the simulation does not. This suggests that there were missing electron-ion recombination reactions or their rates were not fast enough. The electron temperature showed similar behavior where the model matched well in the early portion of the discharge, but the experimental values decayed faster than their model counterparts. As noted before, vibrational excitation of CH_4 was not considered which could accelerate the electron temperature decay at low electron energies.

The model did capture the overall trend of CH_4 addition where for both n_e and T_e, there was a large gap between 0 and 1% CH_4 and a small gap between 1% and 2% CH_4. Since the electron energy is controlled by the reduced electric field (E/N), the time evolution of E/N for the three gas mixtures was plotted in Fig. 3. The modeled E/N showed a distinct drop between 0% and 1% CH_4 while the E/N for 1% and 2% CH_4 looked almost the same. A lower E/N meant electrons gained less energy from the electric field to ionize the neutral gas, which decreased both n_e and T_e. The reason for this drop in E/N could be that the ionization potential of CH_4 is 12.6 eV which is lower than the 24.6 eV ionization potential of He. Therefore, adding CH_4 made breakdown easier and led to earlier establishment of the sheath and self-shielding. Since the breakdown occurred in this case along the rising edge of the voltage pulse, a faster breakdown meant a lower peak electric field and consequently lower electron energies and densities. This effect appeared to be saturated since the E/N did not continue to decrease with doubling the amount of CH_4. Any further differences between 1% and 2% CH_4 came from electron-impact reactions with CH_4 and subsequent charge transfer and electron-ion recombination reactions.

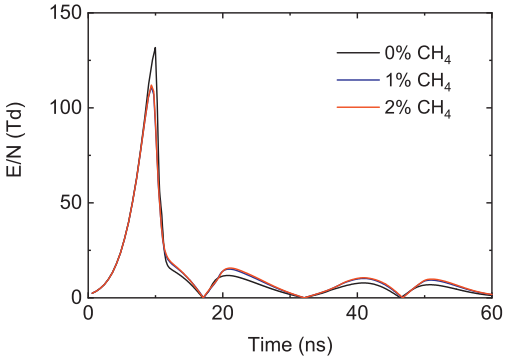

Fig. 3. Time evolution of the reduced electric field (E/N) calculated for 0–2% CH_4 addition to a He ns-DBD.

4.2. Measurements and model predictions of CH_4 pyrolysis and dry reforming

In Fig. 4, the measured temperatures for the pyrolysis and dry reforming mixtures were plotted together with the computed temperature for the $\phi = 1$ dry reforming mixture. The measured

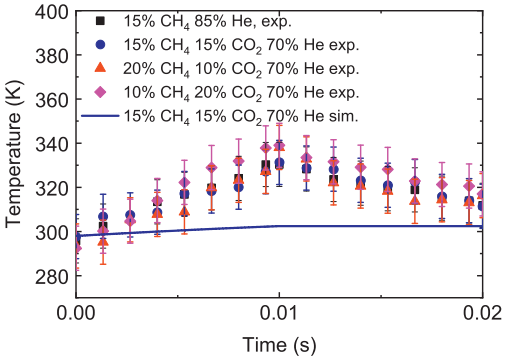

Fig. 4. Measured temperatures of the pyrolysis and dry reforming mixtures and the computed temperature for $\phi = 1$.

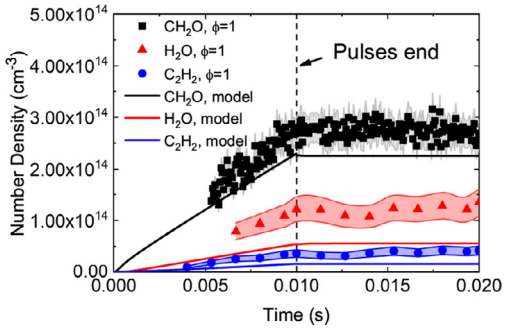

Fig. 5. Measured and predicted time evolution of CH_2O, H_2O, and C_2H_2 in the stoichiometric dry reforming mixture. The dashed line marks the end of the 300-pulse burst.

temperatures all fell within experimental uncertainty of each other. However, the temperature was significantly under-predicted in the model, partially due to the over-prediction of heat loss conducted to the wall via the He bath gas. Additionally, slow heating of the mixture from vibrational to translational mode (V-T) relaxation of CH_4 and CO_2 occurring on tens of microseconds time scale [22] between voltage pulses was neglected in the model and could also contribute to the mismatch. Since the measured temperature rise was only approximately 30K, the modeled kinetics were not significantly impacted. All predicted number densities would be lower if the measured temperature was used, but this discrepancy would be at most 10%.

The measured and predicted species densities are plotted in Fig. 5. The predicted CH_2O profile was close to the measurement uncertainty, while the H_2O and C_2H_2 were under-predicted by a factor of two and three, respectively. This suggests that the pathways for CH_2O were modeled well, but the pathways for H_2O and C_2H_2 were not well-modeled and improved kinetic mechanisms are needed.

To investigate further, the path fluxes for the three measured products in the stoichiometric mixture were plotted in Fig. 6 based on the simulation data. The main production pathways for CH_2O were through the following reactions: $CH_3 + OH \rightarrow CH_2O + H$ and $CH_2 + CO_2 \rightarrow CH_2O + CO$. Given that the predicted time evolution of CH_2O matched fairly well with the experimental data, we conclude that these were the main pathways for CH_2O production. The successful prediction of CH_2O is in contradiction with the previous difficulties with modelling it in plasma-assisted oxidation studies [11,12]. It was previously reported that the CH_2O predictions were highly sensitive to the uncertainties in the branching ratios for the $O(^1D) + CH_4$ reaction. In contrast to O_2, CO_2 mainly dissociates by electron impact into $O(^1S)$ or $O(^3P)$ [23]. Therefore, $O(^1D)$ is not produced in amounts that can influence the kinetics of CH_2O formation in CH_4 dry reforming, which is a fundamental change from the prior oxidation studies.In this work, $O(^3P)$ is considered the main dissociation product since its energy threshold is 7.8 eV versus the 12 eV threshold of $O(^1S)$ [23].

According to Fig. 6, H_2O was mainly produced by reaction of fuel with OH radical. The reaction rate constant used was from Ref. [24] and they reported an uncertainty of 22% at 298K. Therefore, this rate constant could be adjusted within the rate uncertainty but it may not be enough to increase the predicted concentrations by a factor of two. This means that there are additional H_2O pathways not considered in the mechanism.

For C_2H_2, the model predicted several indirect pathways involving multiple intermediate steps that form reactants like C_2H_3, CH_2, and $C_2H_5^+$ before producing C_2H_2. As shown in Fig. 7, CH_3^+ was shown to be significant for the major pathway to form $C_2H_5^+$, and electron-impact reactions with fuel formed the majority of CH_2. Ref. [14] reported high uncertainties in the rate constants: 50%–300% uncertainty for the C_2H_3 reactions and 152% uncertainty for the CH_2 reaction. These rate constants need to be more accurately determined by experiments or theory to improve the prediction. Furthermore, a recent plasma-assisted CH_4 pyrolysis study [25] suggested that the branching ratios for the dissociative electron-impact reactions with CH_4 needed to be updated with significantly more formation of CH_2. Also, reactions of He_2^+ with fuel were included to form additional CH_2 [25], but He_2^+ was not considered in this study. Both of these changes would contribute to increased C_2H_2 production via increased CH_2 (Fig. 6). These modifications could also improve the CH_2O prediction through greater product formation via $CH_2 + CO_2$ (Figs. 6 and 7).

To investigate the effect of the initial mixture composition on the product species formation and selectivity, time-resolved measurements were also conducted for a pyrolysis condition and additional

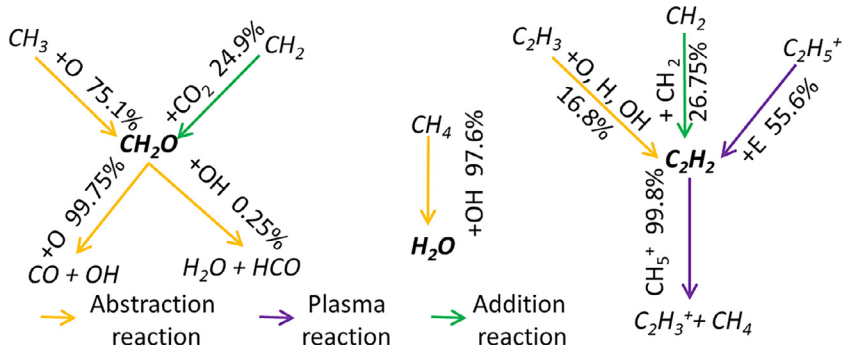

Fig. 6. Production and consumption percentages of the three measured products for the stoichiometric reforming mixture. Percentages on arrows pointing towards and away from the 3 species represent their relative production and consumption fluxes, respectively.

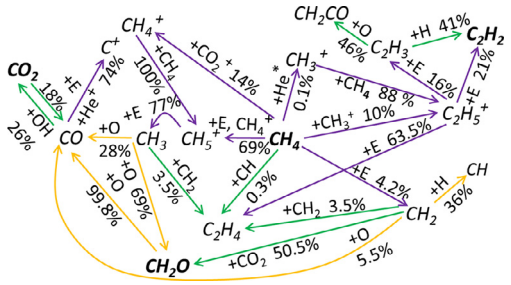

Fig. 7. Path flux analysis of hydrocarbon products for the stoichiometric dry reforming mixture. All percentages are reported as flux from the base of the arrow.

dry reforming equivalence ratios of $\phi = 0.5$ and $\phi = 2$. The experimental measurements for these initial compositions were plotted in Fig. 8. Generally, all three measured product species did not show a strong dependence on equivalence ratio. The greatest contrast was between the dry reforming mixtures and the pyrolysis mixture, where pyrolysis showed a factor of 2 increase in C_2H_2 production. As discussed previously, an important intermediate species for C_2H_2 formation was CH_2. From Fig. 7, half of the CH_2 reacted with CO_2 and formed CH_2O in the $\phi = 1$ case. In the pyrolysis mixture, CH_2 cannot be consumed by CO_2. Hence additional C_2H_2 was produced through CH_2, based on path flux analysis (not shown).

Interestingly, the C_2H_2 concentration in the $\phi = 0.5$ and $\phi = 1$ cases were measured to be very similar. Given the dependence of C_2H_2 production on radicals formed from CH_4 shown in Figs. 6 and 7, this result was unexpected. First, the measured C_2H_2 concentrations had a 20% uncertainty assigned to them, so it was possible that any differences fell into this range. Next, the primary consumer of C_2H_2 was CH_5^+. For fuel richer conditions, the C_2H_2 concentration may be suppressed by the increase in CH_5^+. Indeed, for the $\phi = 2$ case,

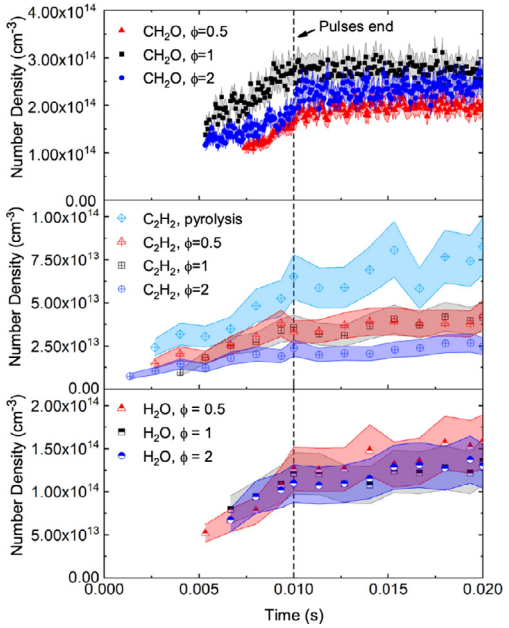

Fig. 8. Measured time evolution of product species for pyrolysis and dry reforming mixtures with ϕ =0.5, 1, and 2. The dashed line marks the end of the 300-pulse burst.

there was a clear drop in C_2H_2 compared with the other equivalence ratios.

For CH_2O, the final measured concentrations in the three mixtures did not vary more than 30% and the maximum production of CH_2O was reached in the $\phi = 1$ case. From Fig. 6, the dominant reaction pathway was from CH_3 + O. Any deviation from stoichiometric conditions would create an imbalance in these radicals as there would be either more CH_3 or more O radical. Additionally, in the model, the primary consumption pathway for CH_2O was its reaction with O radical. Therefore, the $\phi = 0.5$ mixture would have a lower CH_2O concentration

than the $\phi = 2$ mixture, due to enhanced CH_2O consumption by O. This trend was indeed observed for the measured CH_2O shown in Fig. 8.

The experimental H_2O concentrations did not vary dramatically and were within the 20% measurement uncertainty of each other. If CH_4 + OH is the major pathway, then this behavior could be explained. With more CO_2 in the fuel-lean mixture, there would be more O and OH radicals due to an increase in dissociation of CO_2 by electron-impact. That would boost H_2O formation. However, in Fig. 7, CO consumed OH to make CO_2. This reaction has a rate constant that is 500 times larger than that for the CH_4 + OH reaction at 298K. Thus, even CO concentrations of 100 ppm could compete with CH_4 for OH. The H_2O production would drop due to the consumption of OH by CO and limit the variation in H_2O concentration. For the fuel-rich mixture, there would be less CO_2 to produce O and OH, but at the same time, there would be less CO to consume the OH that makes H_2O.

The previous explanations of the equivalence ratio trends assume that the plasma properties were predicted correctly, as they all use pathways involving species like ions and radicals are produced from electron-impact reactions. As shown earlier, changing the mixture can have a nonlinear effect on E/N, n_e, and T_e which would then propagate to the production of these radicals and ions. For example, if the CH_4 ionization, a function of electron energy, was severely under-predicted, then CH_5^+ concentration would also be low, leading to less consumption of C_2H_2 and higher C_2H_2 concentrations. Therefore, it was critical to compare the model against available n_e and T_e measurements to demonstrate its predictive capabilities, but additional measurements are necessary in mixtures with higher reactant mole fractions for complete validation.

5. Conclusion

Use of *in situ* time-resolved diagnostics for measurement of plasma properties and species concentrations was demonstrated to validate predictions of plasma physics and chemical kinetics by a 1-D model of plasma-assisted CH_4 reforming and identify where improvements are needed in the kinetic mechanism. Comparison against the n_e and T_e measurements shows that the nonlinear effect of CH_4 addition on the plasma properties was successfully predicted and the major difference between the 0% CH_4 mixture and 1% CH_4 mixture was due to faster breakdown in the gas. However, the breakdown was not accelerated more by further addition of CH_4, indicating that the comparatively small differences in n_e and T_e were due to changes in electron-impact reactions with CH_4. Time evolution of C_2H_2, H_2O, and CH_2O were measured in pyrolysis and dry reforming mixtures and were used as validation targets for the model. CH_2O was predicted within 25% of the measured values. Path flux analysis for the modelled CH_2O suggests that the primary path for CH_2O production is CH_3 + OH with a secondary path through CH_2 + CO_2. The H_2O and C_2H_2 were under-predicted by a factor of two and three, respectively. From the path flux analysis for these species, more accurate rate constants for reactions involving C_2H_3, CH_2, and $C_2H_5^+$ need to be used for better predictions. Finally, the effect of the "equivalence ratio," defined by the CH_4 dry reforming reaction to H_2 and CO was shown to be weak and this was explained based on the pathways from the stoichiometric dry reforming simulation. These pathways result from radical and ion production initiated through electron-impact which sensitizes the products to uncertainties in the predicted plasma properties. Therefore, combined measurements of both plasma properties and species concentrations are necessary for developing a model with validated plasma physics and chemistry and for obtaining a quantitative understanding of plasma-assisted CH_4 reforming.

Declaration of Competing Interest

The authors declare that they have no known competing financial interests or personal relationships that could have appeared to influence the work reported in this paper.

Acknowledgments

This work was supported by ExxonMobil through its membership in the Princeton E-filliates Partnership of the Andlinger Center for Energy and the Environment. T.Y. Chen is partially supported through the Program in Plasma Science and Technology at Princeton University Fellowship. S. Yang gratefully acknowledges the faculty start-up funding from the University of Minnesota. All simulations were conducted in the Minnesota Supercomputing Institute (MSI). Y. Ju would like to acknowledge the grant support from NSF CBET 1903362, NSF-EFRI grant for distributed chemical manufacturing, DOE DE-SC0020233 of Plasma Science Center, and DOE-NETL DE-FE0026825.

References

[1] L. Wang, Y. Yi, C. Wu, H. Guo, X. Tu, *Angewandte Chemie Int. Ed.* 56 (44) (2017) 13679–13683.
[2] G.G.F.R. Partnership, *The World Bank* (2019).
[3] BP, *BP Stat. Rev. London UK* (2019).
[4] L. Quéré, et al., *Earth Syst. Sci. Data (Online)* 10 (4) (2018).
[5] L. Zhou, B. Xue, U. Kogelschatz, B. Eliasson, *Energy Fuels* 12 (6) (1998) 1191–1199.

[6] M. Scapinello, E. Delikonstantis, G.D. Stefanidis, *Chem. Eng. Process.: Process Intensificat.* 117 (2017) 120–140.
[7] S. Yang, S. Nagaraja, W. Sun, V. Yang, *J. Phys. D: Appl. Phys.* 50 (43) (2017) 433001.
[8] M. Scapinello, L. Martini, G. Dilecce, P. Tosi, *J. Phys. D: Appl. Phys.* 49 (7) (2016) 075602.
[9] X. Wang, Y. Gao, S. Zhang, H. Sun, J. Li, T. Shao, *Appl. Energy* 243 (2019) 132–144.
[10] A. Bogaerts, C. De Bie, R. Snoeckx, T. Kozák, *Plasma Process. Polym.* 14 (6) (2017) 1600070.
[11] J.K. Lefkowitz, P. Guo, A. Rousso, Y. Ju, *Philos. Trans. R. Soc. A: Math. Phys. Eng. Sci.* 373 (2048) (2015) 20140333.
[12] A. Rousso, S. Yang, J. Lefkowitz, W. Sun, Y. Ju, *Proc. Combust. Inst.* 36 (3) (2017) 4105–4112.
[13] S. Yang, X. Gao, V. Yang, W. Sun, S. Nagaraja, J.K. Lefkowitz, Y. Ju, *J. Propul. Power* (2016) 1240–1252.
[14] W. Wang, A. Berthelot, Q. Zhang, A. Bogaerts, *J. Phys. D: Appl. Phys.* 51 (20) (2018) 204003.
[15] T.Y. Chen, A.C. Rousso, S. Wu, B.M. Goldberg, H. van der Meiden, Y. Ju, E. Kolemen, *J. Phys. D: Appl. Phys.* 52 (18) (2019) 18LT02, doi:10.1088/1361-6463/ab0598.
[16] A. Farooq, J.B. Jeffries, R.K. Hanson, *Measur. Sci. Technol.* 19 (7) (2008) 075604.
[17] I.E. Gordon, et al., *J. Quant. Spectrosc. Radiat. Transf.* 203 (2017) 3–69.
[18] S. Yang, V. Yang, W. Sun, S. Nagaraja, W. Sun, Y. Ju, X. Gou, in: Proceedings of the 54th AIAA Aerospace Sciences Meeting, 2016, p. 0195.
[19] G. Hagelaar, L. Pitchford, *Plasma Sources Sci. Technol.* 14 (4) (2005) 722.
[20] A. Kulikovsky, *J. Comput. Phys.* 119 (1) (1995) 149–155.
[21] T. Martens, A. Bogaerts, W. Brok, J. van Dijk, *Anal. Bioanalyt. Chem.* 388 (8) (2007) 1583–1594.
[22] C.B. Moore, *Account. Chem. Res.* 2 (4) (1969) 103–109.
[23] M. Grofulović, L.L. Alves, V. Guerra, *J. Phys. D: Appl. Phys.* 49 (39) (2016) 395207.
[24] A. Bonard, V. Daële, J.-L. Delfau, C. Vovelle, *J. Phys. Chem. A* 106 (17) (2002) 4384–4389.
[25] X. Mao, Q. Chen, C. Guo, *Energy Conv. Manag.* 200 (2019) 112018.